Effect of humidity on granular friction at room temperature

Kevin M. Frye and Chris Marone[1]

Department of Earth, Atmospheric, and Planetary Sciences, Massachusetts Institute of Technology, Cambridge, Massachusetts, USA

Received 1 June 2001; revised 5 April 2002; accepted 9 May 2002; published 20 November 2002.

[1] We report on laboratory experiments designed to investigate the microphysical processes that result in rate- and state-dependent friction behavior. We study the effect of relative humidity (RH) (<5 to 100%) in velocity stepping tests (10–20 μm/s) and slide-hold-slide (SHS) tests (3–1000 s) on 3 mm thick layers of quartz and alumina powders sheared at 25 MPa normal stresses. Granular powders are conditioned in situ under controlled RH to create new surface area before shearing. We find a transition from velocity strengthening to velocity-weakening frictional behavior as RH increases. The transition occurs at 30–35% RH for quartz and 55–60% RH for alumina. Frictional healing is negligible at low humidity and increases with increasing RH for both materials. The coefficient of sliding friction is independent of humidity. We use normal stress vibrations in SHS tests to isolate chemically assisted healing mechanisms operative within contact junctions from compaction induced granular strengthening. We find that reorganization of granular particles influences friction but that chemically assisted mechanisms dominate. Our data show that rate- and state-dependent friction behavior for granular materials, including time-dependent healing and steady state velocity dependence, is the result of chemically assisted mechanisms that can be reduced or turned off at low humidity at room temperature in quartz and alumina. *INDEX TERMS:* 1045 Geochemistry: Low-temperature geochemistry; 5199 Physical Properties of Rocks: General or miscellaneous; 7209 Seismology: Earthquake dynamics and mechanics; *KEYWORDS:* rate- and state-dependent friction, quartz, humidity

Citation: Frye, K. M., and C. Marone, Effect of humidity on granular friction at room temperature, *J. Geophys. Res.*, *107*(B11), 2309, doi:10.1029/2001JB000654, 2002.

1. Introduction

[2] Active faults exhibit a variety of behaviors from stable creep to stick-slip motion. How shearing is accommodated along a fault is determined by the velocity-, slip-, and time-dependence of the frictional strength, which can be described by rate- and state-dependent friction laws. Laboratory studies have led to an understanding that an asperity contact population evolves during shear [*Rabinowicz*, 1951]. Contact junctions strengthen with age [*Rabinowicz*, 1951], possibly through thermally activated mechanisms that increase the contact area [*Dieterich and Kilgore*, 1994, 1996; *Heslot et al.*, 1994] or the contact bonding quality [*Hirth and Rice*, 1980; *Rice et al.*, 2001]. Additionally, the friction behavior of granular materials is a function of shear localization and density changes. Although the empirical rate- and state-dependent laws have been applied successfully to many types of laboratory data and field observations (see *Marone* [1998a] and *Scholz* [1998] for reviews) the precise physical mechanisms responsible for the friction behaviors they describe remain poorly understood. Ideally, laboratory experiments would identify the fundamental, crystal lattice-scale and meso-scale mechanisms of friction under the range of geological conditions relevant to the seismic cycle [*Tullis*, 1988; *Evans and Chester*, 1995]. However, our present understanding of fault material properties together with technical limitations in the laboratory do not allow that level of generality. Instead, in this paper we address the physico-chemical mechanisms responsible for rate- and state-dependent friction effects in quartz and alumina at room temperature. We focus on the fundamental observations on which rate and state friction laws are based: velocity-dependence of steady state sliding friction and time-dependent healing [*Dieterich*, 1972, 1978, 1979; *Ruina*, 1983; *Tullis and Weeks*, 1986; *Chester*, 1994; *Beeler et al.*, 1994; *Marone*, 1998a]. We investigate the influence of water on friction by varying humidity and attempt to separate water-assisted healing from the effects of consolidation and porosity changes in granular layers.

1.1. Influence of Water

[3] Contact-junction strengthening can be achieved through increasing either the quantity of contact area or quality of contact. If asperities on surfaces in brittle frictional contact are assumed to be in a state of incipient

[1]Now at Department of Geosciences, Pennsylvania State University, University Park, Pennsylvania, USA.

0148-0227/02/2001JB000654$09.00

plastic flow [*Bowden and Tabor*, 1964], then time-dependent contact deformation is one possible cause of time- and velocity-dependent friction behaviors. Water is observed to enhance both point defect and dislocation migration in single-crystal quartz, quartz-aggregate, and quartzite systems [*Blacic and Christie*, 1984; *Jaoul et al.*, 1984; *Mainprice and Paterson*, 1984; *Kronenberg and Tullis*, 1984; *Evans and Kohlstedt*, 1995]. Thus water-assisted plastic deformation, commonly known as hydrolytic weakening, could be a mechanism by which the real area of contact grows and the frictional strength of two surfaces increases. If asperities are in purely elastic contact, then time-dependent strengthening can be accomplished through hydrogen bonding [*Rice*, 1976; *Michalske and Fuller*, 1985] or water adsorption/desorption at contact points [*Hirth and Rice*, 1980]. Other possible water-assisted mechanisms of frictional healing are capillary bridging [*Crassous et al.*, 1994; *Iwamatsu and Horii*, 1996], pressure solution [*Dove and Elston*, 1992; *Dove*, 1994; *Bos et al.*, 2000], and subcritical crack growth [*Martin and Durham*, 1975; *Costin*, 1987].

[4] *Dieterich and Conrad* [1984] studied bare quartzite surfaces and found that low humidity conditions resulted in higher values of sliding friction, a lack of time-dependent healing, a switch to velocity strengthening, and greater tendency for stable sliding. Their results imply that hydrolytic weakening influences the friction evolution effect; however the experimental database was small and it was not clear whether water had an effect on steady state velocity-dependence of friction or the friction direct effect. Similar data are not available for granular materials. Thus we study the friction behavior of quartz sand at different humidity levels and examine the relative importance of contact junction processes in determining granular friction behavior.

[5] Alumina serves as a useful comparison since its properties are well documented in engineering literature. In experiments performed with alumina ceramic, *Gates et al.* [1989] found that a weak surface layer was formed in the presence of water during sliding. They interpret the layer as the result of a tribochemical reaction that produces aluminum oxide hydroxide.

1.2. Shear Localization and Granular Reorganization

[6] While the friction behavior of bare surfaces can be thought of in terms of asperity interaction, friction of granular materials is more complex. Grains rotate, break and undergo contact slip, and networks of grains in shear localization fabrics and stress chains influence the frictional properties of granular layers [*Sammis et al.*, 1987; *Wong et al.*, 1992; *Jaeger et al.*, 1996; *deGennes*, 1999; *Geminard et al.*, 1990]. Slip localizes within granular layers (Figure 1), and at normal stresses above the particle strength, localization evolves with displacement. These textural effects and the role of dilation and porosity changes are well documented [*Marone et al.*, 1990; *Segall and Rice*, 1995; *Sleep*, 1997; *Mair and Marone*, 1999]. Yet the role of contact junction processes versus granular reorganization and shear fabric is poorly understood. Theoretical studies of granular friction often employ a strategy where intergranular friction is constant, and the distribution of stress throughout the granular layers is studied [*Mora and Place*, 1998; *Morgan*, 1999; *Morgan and Boettcher*, 1999]. These models indicate that stress is distributed unevenly throughout the granular layer, and that the formation and destruction of load bearing ''stress chains'' play an important role in friction of granular materials.

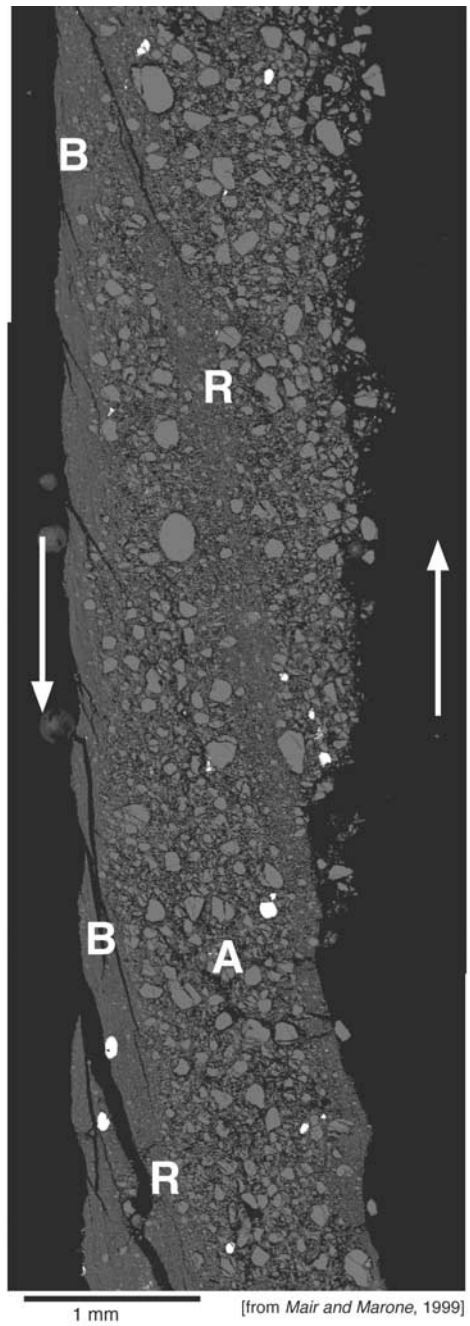

Figure 1. Backscattered electron micrograph of a granular layer after 20 mm of left-lateral shear at σ_n = 50 MPa [*Mair and Marone*, 1999]. Areas of intense comminution are interpreted as boundary (B) and Riedel (R) shears. These zones are surrounded by relatively undisturbed regions (A), where little slip occurs.

[7] In the context of earthquake physics, the above issues bring out an important question. Is the frictional behavior of

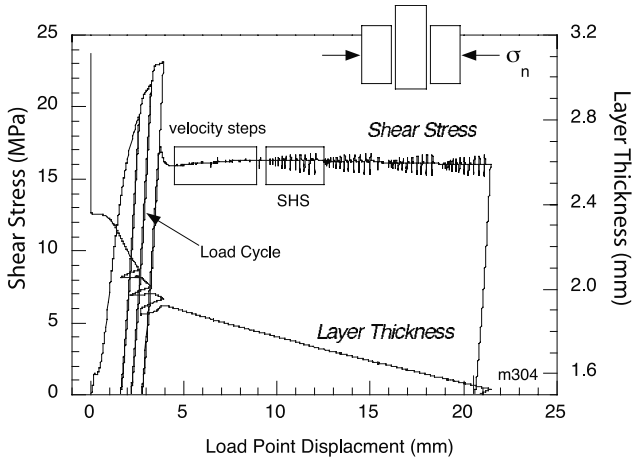

Figure 2. Shear stress and layer thickness history for an entire experiment. Gouge layers are subject to three shear load cycles at high normal stress (40 MPa) to create fresh surface area before velocity stepping tests and SHS tests are carried out at normal stress 25 MPa. Layer thickness decreases throughout the experiment due to comminution and geometric thinning. Superimposed upon this thinning trend are layer thickness perturbations associated with velocity steps and SHS.

gouge-filled fault zones controlled by contact junction processes, the consolidation state of the granular material, or both? Granular materials exhibit much more compaction and dilation during loading perturbations than bare surfaces. *Marone and Kilgore* [1993] and *Sleep et al.* [2000] suggest that the stability and time-dependence of gouge friction is influenced by changes in the thickness of the localized shear zone. Reorganization of the fault gouge during compaction results in more widely distributed shear and smaller strain rates, and may be modeled with the rate- and state-dependent constitutive laws if velocity is expressed in terms of strain rate.

[8] We propose that frictional healing between slip events under ambient laboratory conditions is a function of both granular consolidation and water-assisted, time-dependent strengthening of contact junctions. We perform experiments as a function of relative humidity (RH) to alter the kinetics of contact junction strengthening processes. We find that healing behavior varies significantly as a function of RH for both quartz and alumina powders, while compaction and dilation show less variation, and thus, we infer that rate and state friction behavior is due to chemically assisted contact junctions processes.

2. Experiment Procedure

[9] All laboratory experiments in this study were performed in a double-direct shear apparatus (for details, see *Marone* [1998a] and *Karner and Marone* [2000]). In this configuration, two frictional surfaces are sheared simultaneously (Figure 2, inset). Shear load was applied as a vertical displacement or rate boundary condition by servo-control with 0.1-μm-resolution. The horizontal ram applied normal force in load-feedback mode with 0.1 kN resolution. Position and applied force are measured at each load point at a sampling rate of 1 to 10 kHz. The raw data is averaged and recorded at 1 to 10 samples/s.

2.1. Apparatus and Materials

[10] Test samples consisted of 3-mm-thick layers of quartz or alumina powder sheared between rough steel forcing blocks. Grooves were machined perpendicular to the shear direction to eliminate slip at the layer boundaries and confine shear within the granular layers. The nominal area of contact was constant at 10×10 cm^2 during tests.

[11] The quartz powder was subangular Ottawa sand, which is >99% SiO_2, as supplied by the U.S. Silica Co. We used Natural Grain product F-110, which has an initial median particle size of 110 μm and a size range of 50–150 μm. The quartz powder was heated in a vacuum oven to 110°C to remove excess surface water. The alumina was of 95% purity, with an initial mean particle size of 122 μm, a size range of 100–150 μm, and was not oven dried. Significant crushing occurs during shear, such that the mean particle size is <10 μm during steady state frictional shear.

[12] Gouge layers were constructed in a leveling jig to ensure that layers were uniform and reproducibly 3.0 mm thick. Cellophane tape was used to confine layer edges during construction, which was carried out on the side (sample) blocks. The three-block sample (see inset to Figure 2) was assembled by placing the center block on top of one gouge layer and side block, securing this with tape, and then positioning these two blocks on the second side block. When this configuration was secured with tape, steel plates were fastened to the side blocks to cover the front and rear layer edges and thin copper shims were added below each layer to reduce gouge loss during shear. The steel plates made a zero-load sliding contact with the center forcing block, which was coated with MoS_2 lubricant to reduce friction. The base of the copper shims and side blocks and the top of the center block were also lubricated to allow lateral motion during shear.

2.2. Experiment Technique

[13] The test sample and loading system were isolated from room atmosphere with a flexible membrane and RH was varied from <5 to 100% (Table 1). Depending on the desired experiment humidity, a desiccator or a humidifier was placed in the test chamber with the sample and a hygrometer. To allow the granular layer to equilibrate at a given humidity, unsaturated samples were held in the controlled humidity environment for 12 hours before normal load was applied. Saturated experiments were performed by wrapping the sample assembly in latex, applying a small normal force, and adding water or brine until the jacket was filled. Thus the granular layers were fully submerged in these experiments.

[14] After samples equilibrated in the controlled humidity chamber, normal stress σ_n was raised to 40 MPa and three shear load cycles were performed to enhance grain crushing and produce new surface area in situ (Figure 2). Normal stress was then reduced to 25 MPa and shearing was carried out at a rate of 10 μm/s. To further condition the gouge layers and establish a steady state friction level, we performed velocity stepping experiments for the displacement

Table 1. Experiments[a]

Experiment	Powder	Humidity, %	Saturating Solution	σ_n Oscillations (Double Amplitude)
m304	quartz	55	···	···
m307	quartz	5	···	···
m308	quartz	8	···	···
m309	quartz	25	···	···
m310	quartz	60	···	···
m311	quartz	10	···	···
m312	quartz	5	···	···
m314	quartz	4 → 100	DI water	···
m318	quartz	45	···	···
m321	quartz	88	···	···
m340	quartz	45	···	2A = 3.55 MPa
m341	quartz	4	···	2A = 3.53 MPa
m377	quartz	100	DI water	···
m378	quartz	100	1 *M* NaCl	···
m404	alumina	25	···	···
m424	alumina	100	tap water	···
m427	alumina	75	···	···
m430	alumina	41	···	···
m432	alumina	45	···	···
m434	alumina	52	···	···
m435	alumina	86	···	···
m436	alumina	66	···	···
m438	alumina	5	···	···
m450	alumina	100	DI water	···
m453	quartz	100	0.1 *M* NaCl	···

[a] All experiments were performed at $T = 24°C$ (±1.5°C).

range 5–9 mm. SHS tests were performed for the displacement interval form 9 to 13 mm.

2.3. Gouge Preconditioning and Surface Area

[15] Since it is not possible to reliably vary RH within a given experiment, different experiments must be compared. In order to resolve the effect of humidity on second-order friction behavior, we found that gouge layers had to be ground in situ under controlled RH and that initial layer thickness, displacement history, and normal stress history had to be identical in all experiments. Comminution was enhanced by the load cycles at high normal stress (Figure 2). This also helped to localize shear and resulted in steady state friction being reached in less net displacement than without the load cycles.

3. Data and Observations

[16] We use SHS tests to assess the effect of humidity on static friction and time dependent frictional restrengthening. Following the methods of *Dieterich* [1972], *Beeler et al.* [1994], and *Marone* [1998b] the load point is stopped for periods of 3–1000 s after which loading resumes and "static" friction is measured (Figure 3). Because of the frictional rheology and finite stiffness of the testing apparatus, frictional creep occurs during holds (Figure 3a). When the vertical ram is restarted at the initial driving velocity, hardening occurs until frictional yield strength is overcome and then friction returns to steady state sliding. The difference between the peak and steady state sliding friction is defined as healing ($\Delta\mu$). We focus on SHS tests in the shear displacement range of 9 to 13 mm (shear strains of four to seven) for this study.

3.1. Effect of Humidity on Frictional Healing

[17] Figures 3a and 3b show SHS data for an experiment conducted at 55% RH. SHS tests conducted at lower humidity are qualitatively different (Figure 3c). Frictional creep ($\Delta\mu_c$) is greater during low humidity holds, and peak friction is smaller than corresponding tests at higher humidity. The low humidity experiments exhibit negligible healing and little to no time dependence of $\Delta\mu$.

[18] Humidity step tests [*Dieterich and Conrad*, 1984] were performed to check that humidity effects are independent of net shear strain or other minor effects that may vary between experiments (Figure 4). For these tests we began with the procedure for a low humidity run and then opened the test chamber and added water directly to the granular layers, raising RH to 100%. Figure 4 shows that SHS tests performed immediately after adding water dem-

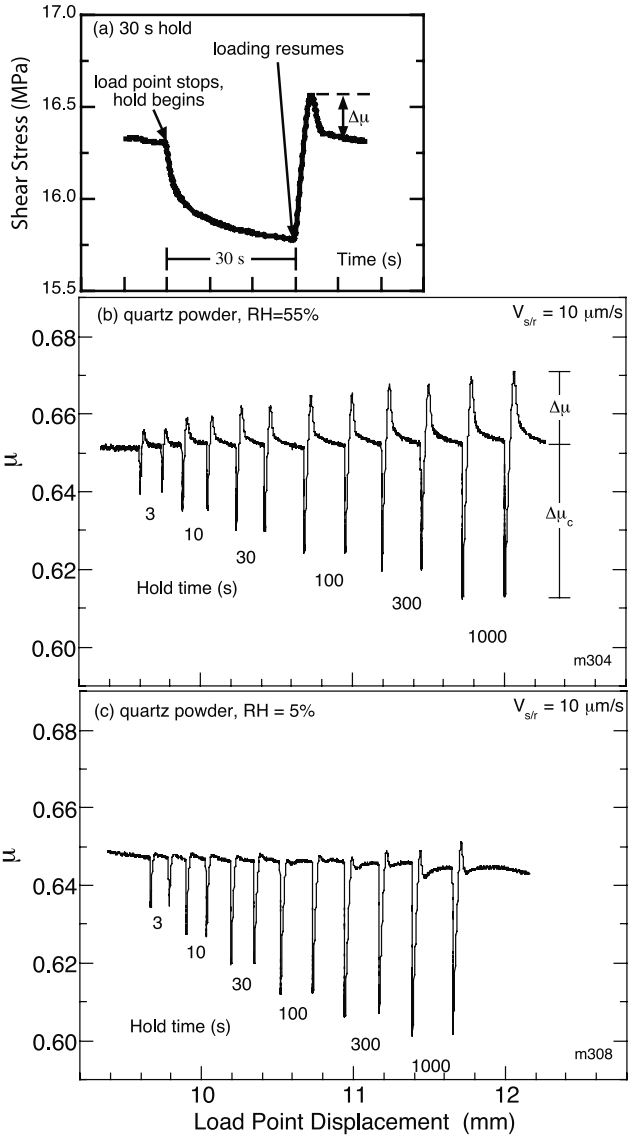

Figure 3. SHS tests for quartz powder. (a) Typical 30 s hold shows frictional creep when load point stops and stress peak when loading resumes. (b) Typical set of SHS tests performed at 55% RH illustrate frictional creep ($\Delta\mu_c$) and frictional healing ($\Delta\mu$). (c) Under dry conditions, with the same displacement history shown for panel b, healing is negligible.

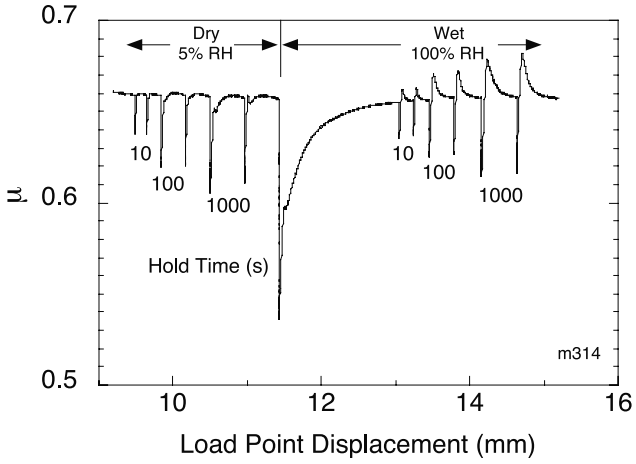

Figure 4. Humidity step test showing the effect of adding water to a low RH experiment. Healing is negligible under dry conditions, but after water is added distinct frictional peaks and time-dependent healing are observed.

onstrate high-humidity behavior; thus humidity effects are not coupled with net displacement or other factors related to gouge zone microstructure.

3.1.1. Quartz Powder

[19] Figure 5 shows the systematic friction behavior for quartz powder at four values of RH. At low humidity, frictional peaks are very small after holds, and there is little time dependence. At 25% RH, frictional peaks are observable after holds, and they evolve over a finite displacement back to steady state sliding friction. As RH increases, healing rates and the evolution distance increase.

3.1.2. Alumina Powder

[20] While quartz powder begins to display some time-dependent healing at RH >5%, alumina powder does not exhibit significant healing for RH up to 50% (Figure 6). Both the qualitative and quantitative character of frictional healing of alumina varies with RH. At low humidity, SHS tests do not exhibit a clear friction peak, instead evolving gradually back to steady sliding. The frictional behavior at 5% RH indicates negligible strengthening during quasi-static holds, allowing sample slip earlier during reloading. Net healing is zero at 25% RH (Figure 6) and data resemble quartz powder at 5% RH (both healing rate and evolution distance are near zero). With increasing RH, peak friction increases and the evolution distance decreases. For both alumina and quartz, creep relaxation during holds is independent of humidity.

[21] SHS tests show that several aspects of frictional restrengthening vary systematically with humidity. We show healing data for a given hold time as a function of RH in Figure 7. For quartz, $\Delta\mu$ increases rapidly at low humidity and saturates at roughly 50% RH. Alumina powder exhibits no observable healing until 45–50% RH. Healing increases with humidity from 50 to 100%. Four

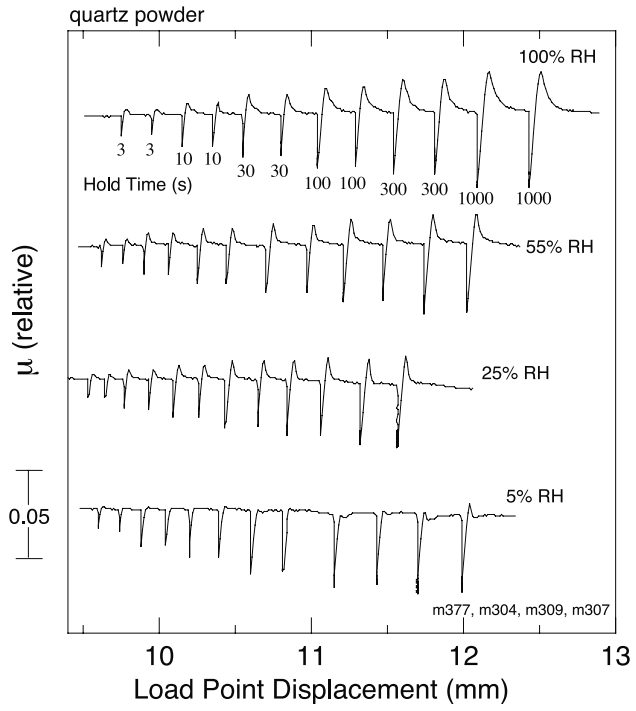

Figure 5. Data from four experiments on quartz powder performed at different values of RH. The same sequence of hold times, labeled on the 100% RH test, were used in each experiment. Friction is offset vertically for clarity. The low humidity tests exhibit little healing. Healing rates increase with humidity and approach a constant value above 55%. The evolution distance needed to reach steady state sliding after a hold increases with RH.

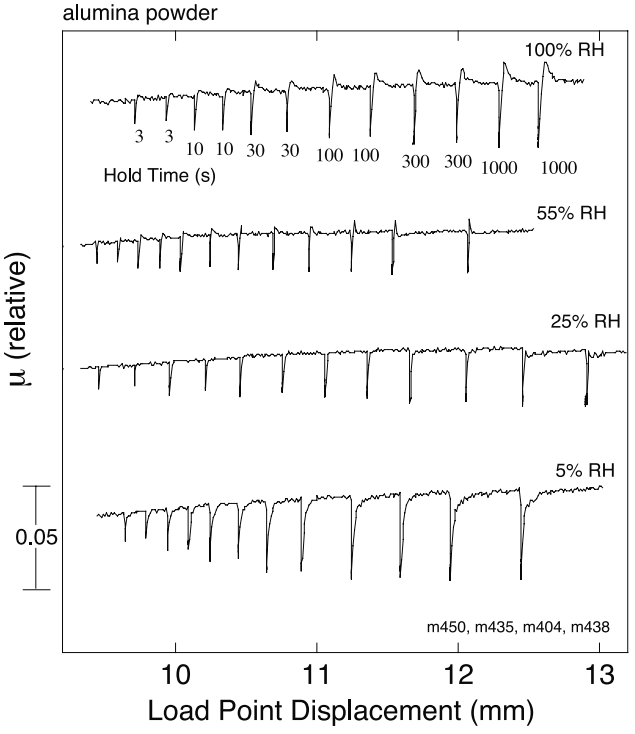

Figure 6. Data from four experiments on alumina powder performed at different values of RH. The same sequence of hold times, labeled on the 100% RH test, were used in each experiment. Friction is offset vertically for clarity. The low humidity tests exhibit little healing. Frictional peaks become measurable above 50% RH. The evolution distance needed to reach steady state sliding after a hold is negligible for the intermediate RH cases.

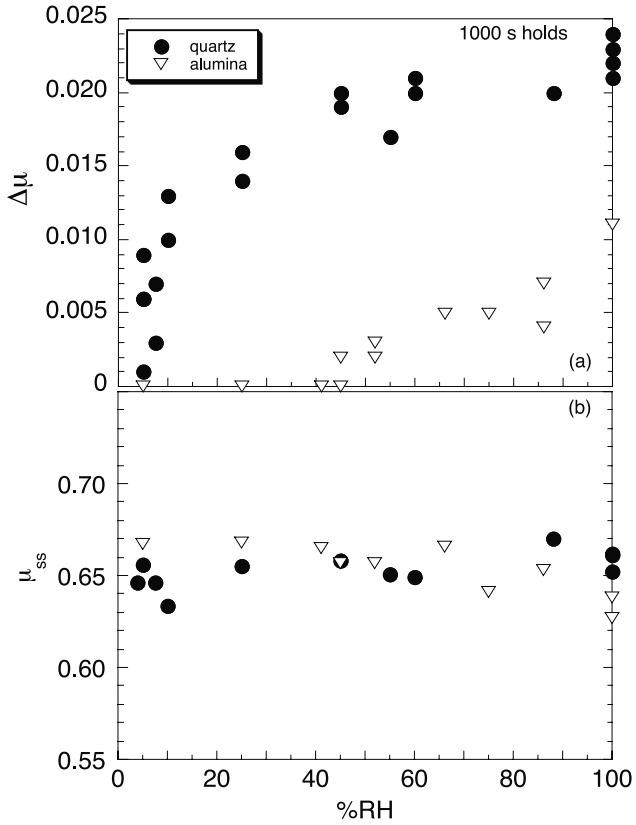

Figure 7. (a) Comparison of healing ($\Delta\mu$) measured after 1000 s holds for both quartz and alumina powders as a function of RH. Healing increases dramatically for quartz from 5–25% RH and then approaches a constant value above 55% RH. Alumina exhibits negligible healing for RH <50% and much less healing than quartz for all humidities. Data points from three saturated (100% RH) alumina powder experiments have the same value and plot over one another. (b) The steady state coefficient of sliding friction measured at 9.5 mm (μ_{ss}) is remarkably consistent through the entire range of measured RH. Experimental reproducibility for a given humidity is high because great care is taken to prepare identical samples and each experiment is run with identical shear displacement and normal stress history.

data points from two alumina experiments overlap at 100% RH. Although healing varies with humidity, the steady state coefficient of friction is remarkably consistent, independent of RH. This result differs from the findings of *Dieterich and Conrad* [1984], who observed a strong humidity dependence of μ_{ss} in their work on bare quartzite surfaces without gouge. The RH-dependence observed by Dieterich and Conrad could be due to lower experimental humidity in their "dry" case, or bare surfaces could be fundamentally different from powders. Numerical studies of granular friction [*Morgan*, 1999; *Thornton*, 2000] indicate that sliding friction of granular systems is nearly independent of inter-particle friction, thus we favor the latter interpretation.

3.2. Layer Thickness Changes

[22] We made high-resolution measurements of layer thickness changes during SHS tests in order to assess the role of compaction and granular densification in healing. Figure 8 shows an example of the relationship between frictional strength and layer thickness during a 30 s SHS test. A linear trend has been removed from the thickness data to account for geometric layer thinning (Figure 2). Layer thickness decreases during the hold until loading resumes. At that point, dilation occurs until peak static strength is reached. The magnitude of dilation is less than compaction, indicating that SHS tests result in an increment of irrecoverable compaction. Previous work on quartz powders by *Karner and Marone* [2001] suggests that this net compaction occurs outside of zones of localized shear.

[23] Figure 9 shows a comparison of healing and compaction data from a suite of tests on quartz. Healing rate $\beta = \Delta\mu/\log_{10} t_h$ increases systematically with increasing humidity. Compaction increases linearly with log hold-time, even when healing is negligible (Figure 9b). A similar response occurs for alumina (Figure 10). We find that healing rate increases systematically with increasing humidity, while compaction in alumina powders does not vary greatly with humidity. Systematic variations in creep ($\Delta\mu_c$), compaction, and dilation are evident in both quartz and alumina experiments (Figure 11), but these variations do not correlate with

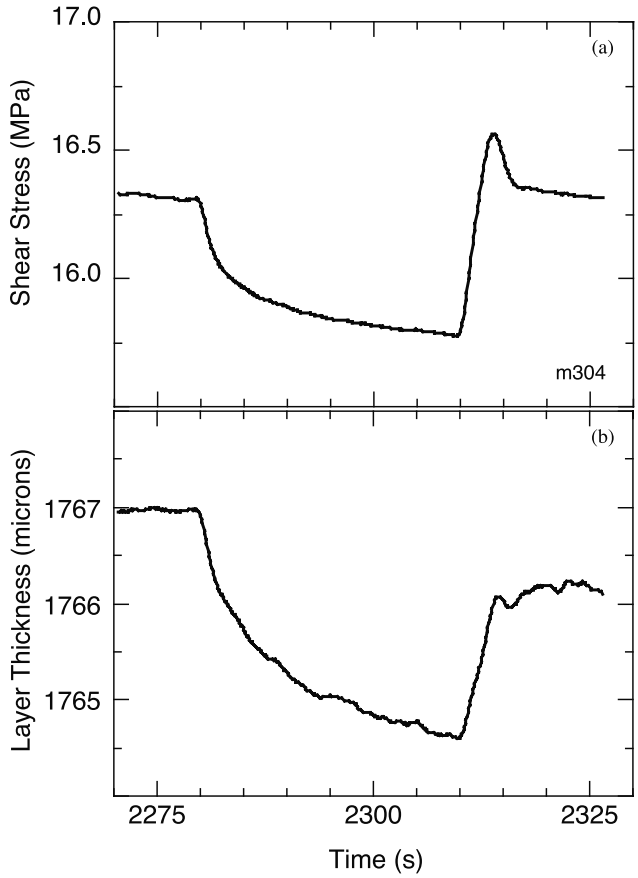

Figure 8. (a) A 30-s SHS test from Figure 3a is shown with (b) corresponding layer thickness change. Compaction occurs during the hold as shear stress relaxation occurs. When loading resumes, the layer dilates to accommodate displacement.

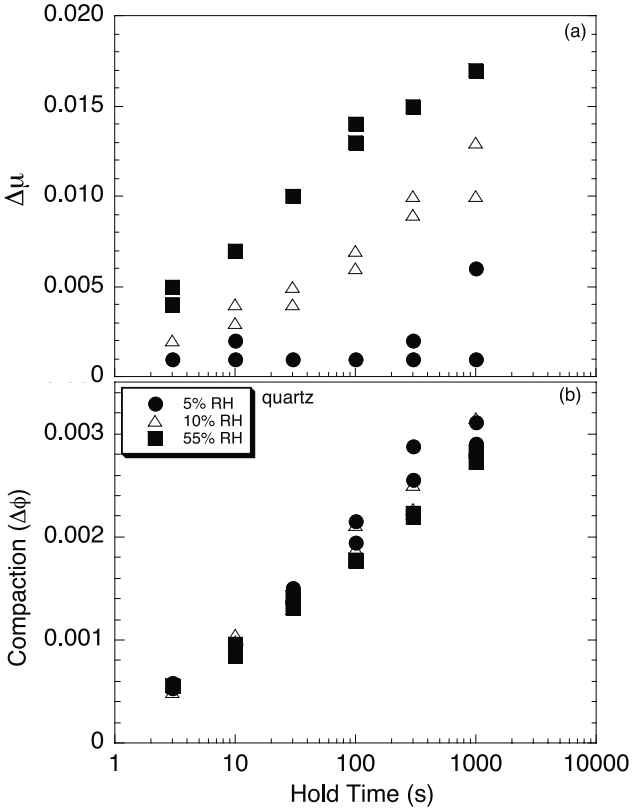

Figure 9. (a) Three representative sets of healing data for quartz powder. Healing is negligible at 5% RH, and increases with increasing RH. (b) Compaction proceeds linearly with log hold time and is independent of RH. Compaction is defined as change in layer thickness during the hold divided by layer thickness before the hold.

the healing data. SHS dilation is consistently less than SHS compaction and thus, net compaction (Figure 8) occurs for the entire range of conditions studied.

3.3. Normal Stress Oscillations

[24] Although we are able to eliminate frictional healing at low humidity without changing the compaction signal (Figures 9 and 10), *Richardson and Marone* [1999] show a correlation between compaction and frictional healing. Their tests were performed at room temperature and humidity, and applying normal stress oscillations during quasi-static holds varied compaction. To investigate these observations further, we perform similar normal stress oscillations during SHS tests (Figure 12) at low and high RH, using the technique of Richardson and Marone. When the shear load point was stopped, a 1 Hz periodic oscillation signal was summed with the normal load servo-control signal. The signal was ramped to its peak amplitude (3.53–3.55 MPa) at the beginning of the hold and rapidly ramped down at the end of the hold. The ramps were employed to reduce instabilities that are common to fluctuating normal stress experiments [*Richardson and Marone*, 1999; *Boettcher and Marone*, 2001].

[25] Normal stress vibrations resulted in greater healing relative to constant normal stress experiments at both low and high humidity (Figure 13). For a given hold time, vibration increased compaction by a factor of 2 relative to constant normal stress tests. Low humidity healing is non-zero but less than 45% RH healing in vibrated SHS tests. At low humidity, there is a change in healing rate at about 100 s, suggesting that the healing mechanism saturates at relatively short timescales for dry conditions.

3.4. Velocity Stepping Tests

[26] Velocity stepping experiments were performed from 5 to 10 mm displacement in all experiments and again from 13 to 15 mm displacement in alumina experiments. Load point velocity was alternated from 10 to 20 μm/s and sliding occurred at each velocity until a new steady state value of friction was reached. In general, the friction response we observed was similar to previous work [e.g., *Dieterich*, 1979, *Marone*, 1998a].

[27] For quartz powder under dry conditions (≤25% RH), μ_{ss} increased with increasing velocity, indicating velocity-strengthening behavior (Figure 14). There is a transition to velocity weakening behavior with increasing humidity. The behavior of alumina powder is similar to that of quartz (Figure 15), but the degree of velocity strengthening at low RH is much greater for alumina than for quartz.

[28] The velocity dependence of steady state friction ($a-b$) [*Dieterich*, 1978, 1979; *Ruina*, 1983], is taken directly from velocity stepping data (Figure 14). The parameter ($a-b$) changes from velocity strengthening to velocity weakening

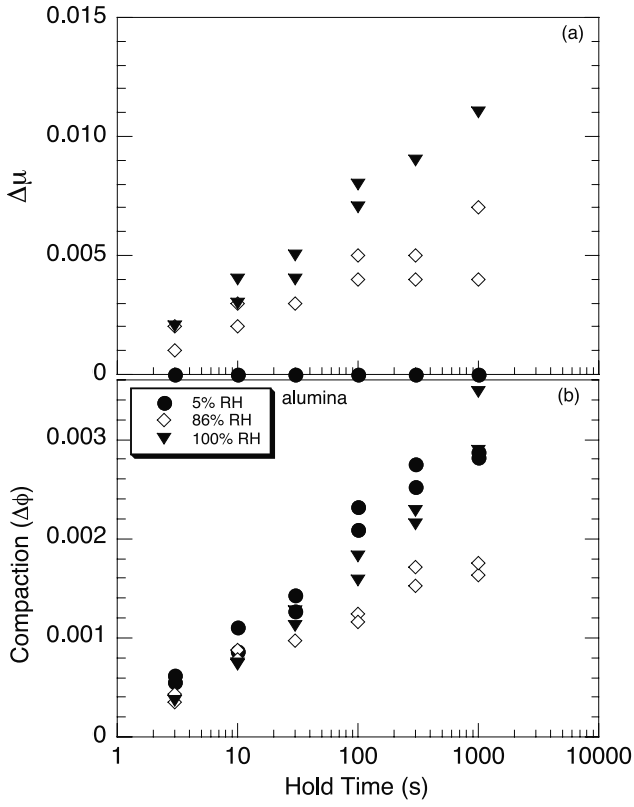

Figure 10. (a) Three representative sets of healing data for alumina powder. Healing is negligible at 5% RH, and increases with increasing RH. (b) Compaction proceeds linearly with log hold time and is independent of RH.

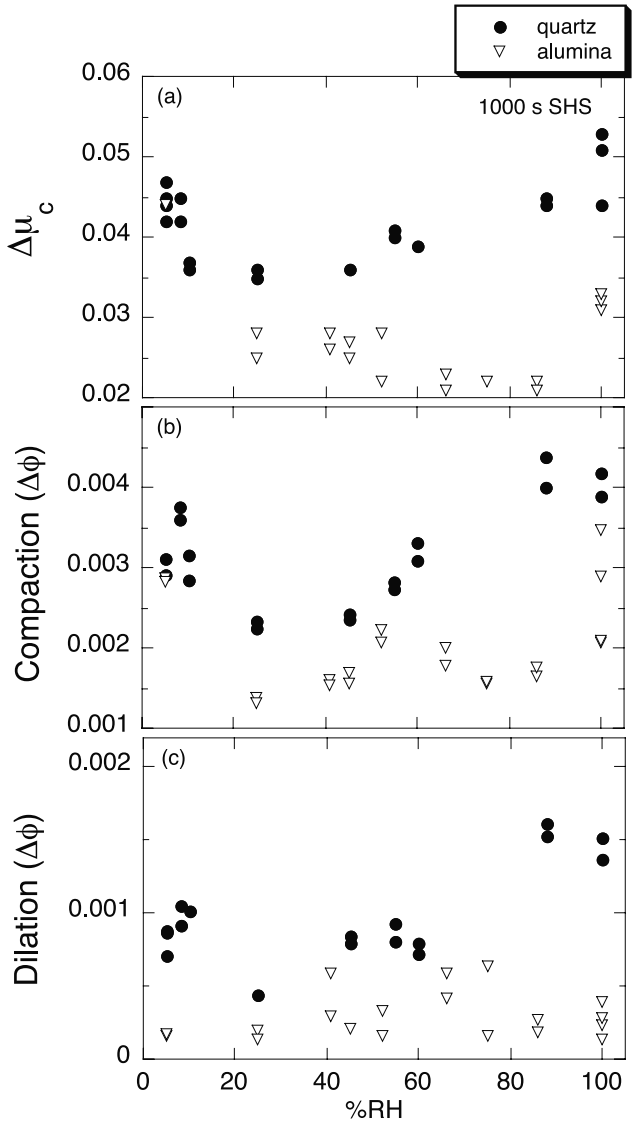

Figure 11. (a) $\Delta\mu_c$, (b) compaction, and (c) dilation all vary with RH for both alumina and quartz. The largest values for creep, compaction and dilation occur at very low and very high RH.

at ~35% RH for quartz powder and ~65% RH for alumina powder (Figure 16). The variation of velocity dependence with humidity is much greater for the alumina powder than for quartz. Figure 17 shows representative constitutive parameters for our range of experimental conditions. The velocity stepping data were modeled using the Dieterich formulation for rate- and state-dependent friction:

$$\mu = \mu_0 + a \ln\left(\frac{V}{V_0}\right) + b \ln\left(\frac{V_0\theta}{D_c}\right), \quad (1)$$

$$\frac{d\theta}{dt} = 1 - \frac{V\theta}{D_c}, \quad (2)$$

where μ is the friction at sliding velocity V, μ_0 is the friction at reference velocity V_0, θ is the state parameter, D_c is the evolution distance, and a and b are empirical constants. We use an iterative, nonlinear, least squares inversion. For quartz, we find that the friction parameter a (direct effect) decreases with increasing humidity, approaching a constant value after 25% RH. The evolution term b increases with increasing RH, and D_c decreases as RH increases. For alumina, the parameters a and b decrease with increasing RH to minimum values at 86% RH, but are dramatically larger at 100% RH. Evolution distance D_c decreases with increasing RH from very large values at low RH (Figure 17). The measured values of a and b are comparable to those measured by *Tullis and Weeks* [1986] for granite bare surfaces, while D_c is larger for our granular samples.

4. Discussion

4.1. Mechanisms of Frictional Aging

[29] Compaction and dilation of granular layers are greatest at very low and very high RH (Figure 11). Reduced time-dependent strengthening may increase compaction at low RH; the mechanism responsible for enhanced compaction at high RH is unclear. The RH-dependence of compaction and dilation does not appear to be related to frictional healing (Figures 9 and 10), precluding the use of entirely

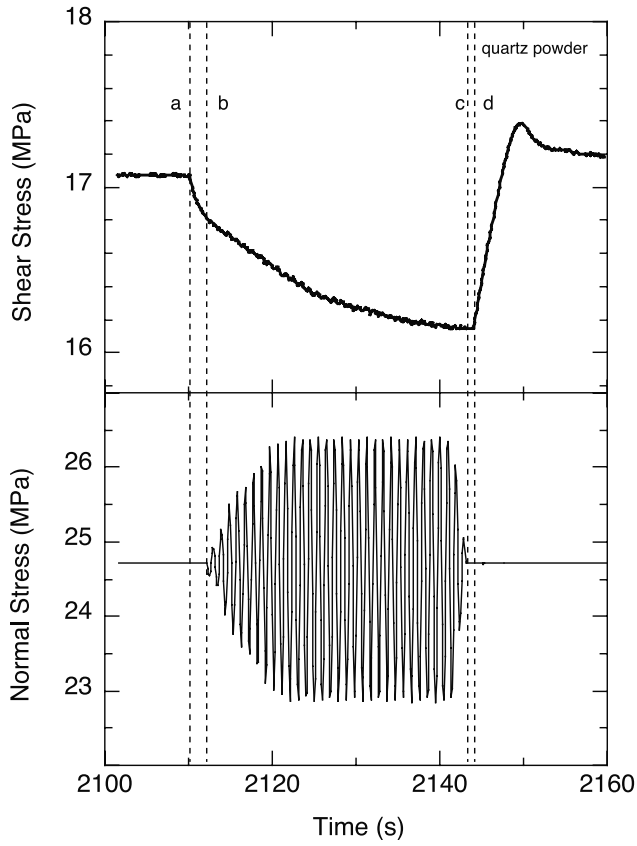

Figure 12. Shear stress and normal stress versus time for a quartz-powder SHS test with normal stress oscillations. Fiducial lines mark where the load point stops (line a), oscillations begin (line b), oscillations stop (line c), and shear loading resumes (line d). Note that oscillation amplitude increases gradually over roughly a 5-s interval.

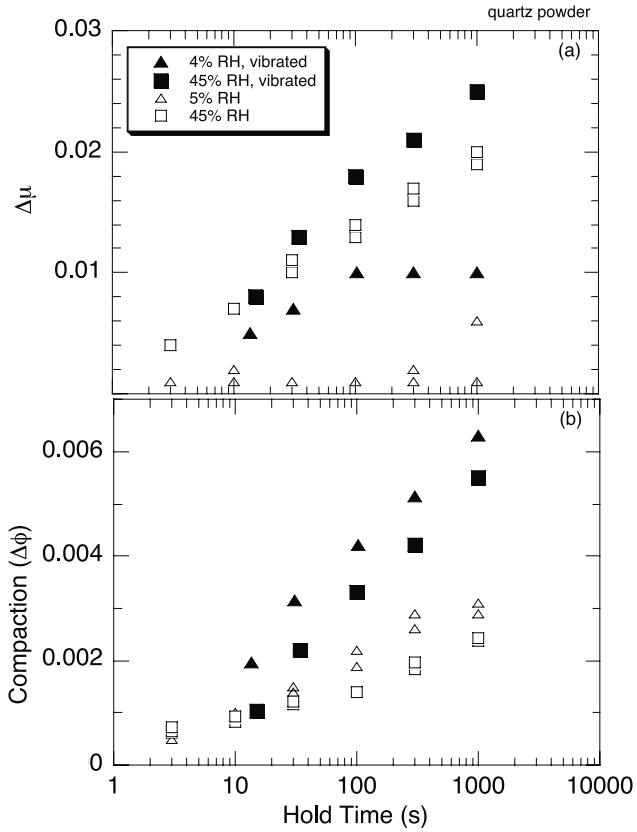

Figure 13. (a) Healing versus hold time for vibrated and constant normal stress SHS tests (quartz powder). Data from vibrated tests show greater healing than constant normal stress tests at a given humidity. In the dry tests, vibration enhanced healing becomes constant for hold times greater than 100 s. (b) Compaction during normal stress vibration tests are approximately double those of constant normal stress tests.

mechanical packing arguments to explain the observed healing data and its RH dependence.

[30] Our observations show that time-dependent frictional healing can be reduced or eliminated at low RH. Healing rates for quartz powder approach a constant value above 50% RH, while frictional healing rates in alumina are at a maximum under saturated conditions. These observations suggest a water-assisted, time-dependent healing mechanism that can effectively be turned off at low RH. Possible water-dependent mechanisms include capillary bridging, pressure solution, hydrolytic weakening of contacts, elastic weakening due to subcritical crack growth, desorption of water at contacts, and hydrogen bonding between adsorbed water.

4.1.1. Quartz Powder

[31] Capillary bridging is a process through which surface water connects and adheres solids and enhances frictional aging in low normal stress applications. Bridging is a time-dependent, thermally activated process [*Bocquet et al.*, 1998] and is important in systems such as sandpiles [*Hornbaker et al.*, 1997; *Halsey and Levine*, 1998]. However, the strength of capillary bridges is small compared to the expected contact stresses for quartz of 1–10 GPa [*Scholz and Engelder*, 1976; *Teufel and Logan*, 1977; *Boitnott et al.*, 1992; *Dieterich and Kilgore*, 1996]. Moreover, if capillary bridging were important, we would expect to see a discontinuity in healing rate at 100% RH because bridges do not form under saturated conditions on quartz. Instead, we observe that frictional aging is continuous as a function of RH through saturated conditions.

[32] We varied the salinity of the saturating solution from distilled water to 1 M NaCl in a suite of 100% RH experiments. Even at room temperature, that variation should be enough to change the dissolution rate for quartz by orders of magnitude [*Dove and Elston*, 1992; *Dove*, 1994]. However, there was little healing variation observed in the 100% RH experiments. Therefore, it is unlikely that dissolution-controlled processes such as pressure solution are responsible for increasing the real area of contact at grain-grain contact junctions.

[33] Reduction of elastic stiffness due to subcritical crack growth is a possible means through which real area of contact could grow. However, it is unclear that large changes in stiffness could be attained in the very localized regions about asperities. Further, with displacement and comminuting, shear zones contain smaller grains with smaller flaws. Therefore, subcritical crack growth should become less effective as a healing mechanism with reduction of average grain size. This is inconsistent with

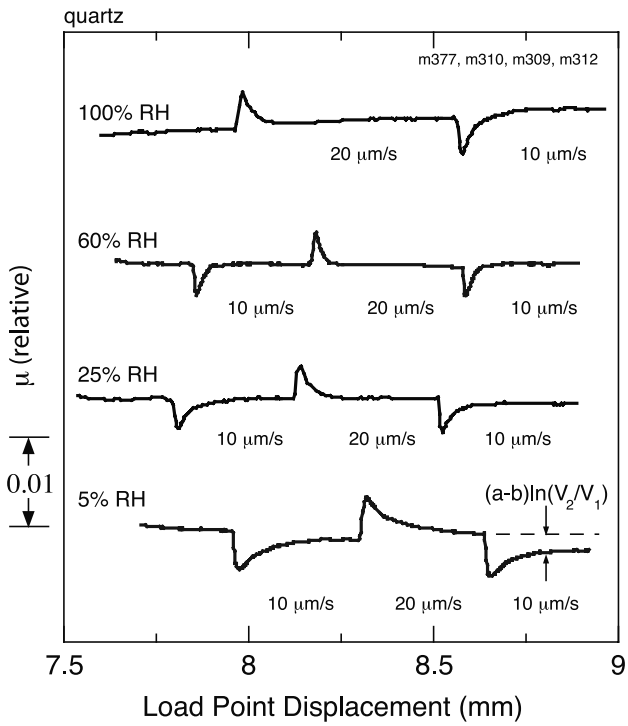

Figure 14. Four sets of quartz powder velocity-stepping tests performed at different values of RH. Friction data are offset vertically for clarity. The low humidity tests demonstrate velocity strengthening. At 8.5–9 mm displacement, quartz powder becomes velocity neutral at 60% RH and velocity weakening at 100% RH.

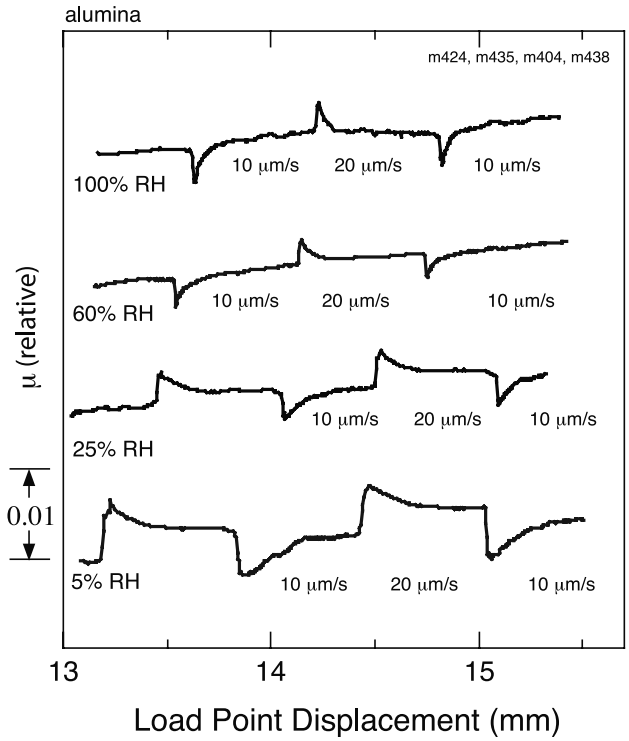

Figure 15. Four sets of alumina powder velocity-stepping tests performed at different values of RH. Friction data are offset vertically for clarity. The low humidity tests demonstrate velocity strengthening. At 14–15 mm displacement, alumina powder becomes velocity neutral at RH >60% and velocity weakening at 100% RH.

observations that healing rate increases with net shear displacement [*Richardson and Marone*, 1999].

[34] We propose that the humidity dependence observed in our experiments is due to adsorption of water onto the surfaces of quartz particles. The water could enable hydrolytic weakening and contact area growth, or time-dependent contact strengthening through either hydrogen bonding or desorption mechanisms [*Hirth and Rice*, 1980; *Dieterich and Conrad*, 1984; *Michalske and Fuller*, 1985]. The

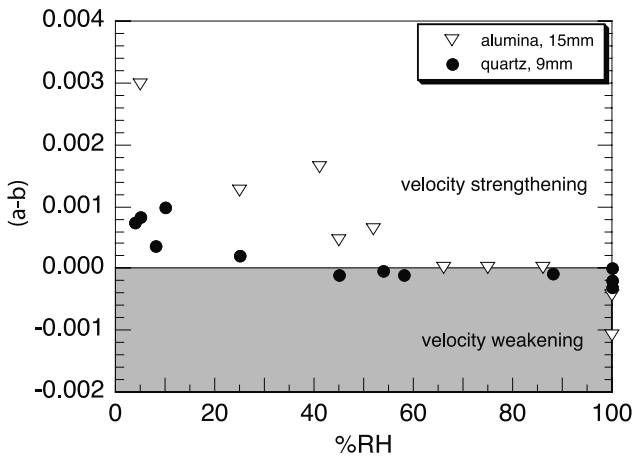

Figure 16. Friction exhibits velocity strengthening behavior at low humidity for both quartz and alumina powders. A transition to velocity neutral or velocity weakening behavior occurs at ≈35% RH for quartz and ≈65% RH for alumina. Alumina exhibits a greater humidity dependence of $(a-b)$ than quartz.

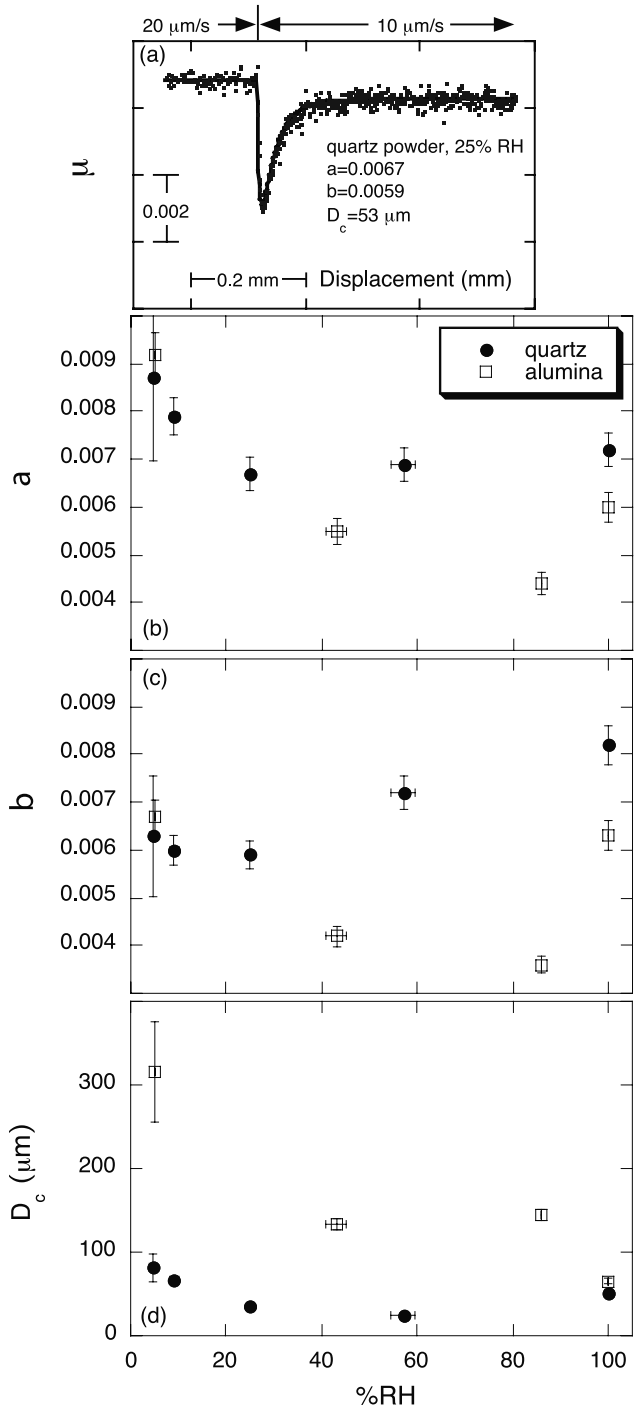

Figure 17. The velocity dependence of quartz and alumina powder was modeled using the *Dieterich* [1978, 1979] formulation of the rate- and state-friction law. (a) Raw data and model fit for a 20–10 mm/s velocity step shown for quartz powder at 55% RH. (b) The model parameter a is plotted versus RH for alumina and quartz samples. (c) The model parameter b is plotted versus RH at the same scale as Figure 17b. (d) The parameter D_c, the evolution distance, is plotted versus RH.

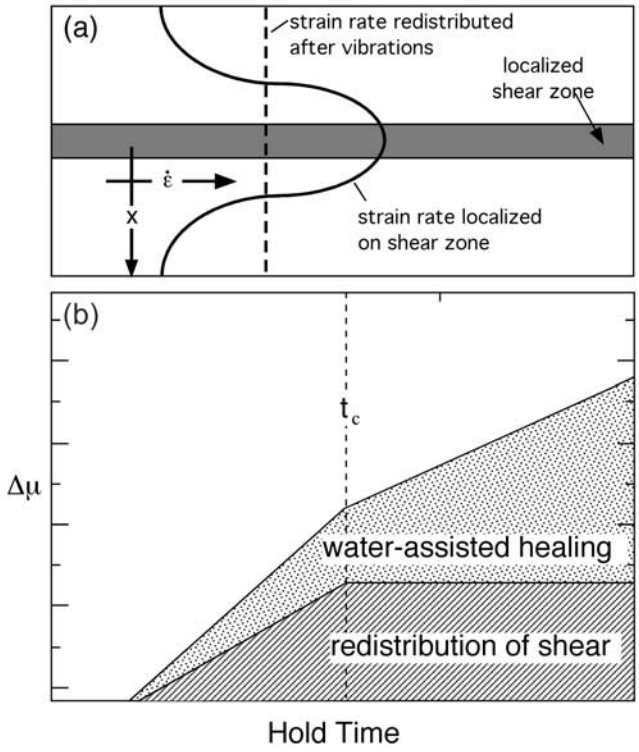

Figure 18. (a) Schematic diagram showing an idealized granular layer with a region of localized shear [after *Sleep et al.*, 2000]. Strain rate is highest within the localized zone. Normal stress vibration during holds disrupts strain rate localization and effectively delocalizes shear. This cartoon shows the idealized case of complete strain rate delocalization during a vibrated SHS test. (b) A schematic interpretation of humidity-dependent healing in SHS tests (e.g., Figure 12). For a granular layer of finite thickness, a critical time (t_c) is needed to redistribute shear at a given vibration amplitude and frequency. Therefore, for dry conditions, healing due to shear redistribution saturates for hold times greater than t_c. At moderate humidity, an additional water-assisted healing mechanism produces increased healing.

frictional healing rate of quartz becomes nearly constant at RH >50%, which is the humidity at which quartz surfaces become completely covered with a water monolayer [*Whalen*, 1981; *Michalske and Fuller*, 1985].

4.1.2. Alumina Powder

[35] *Gates et al.* [1989] found layers of weak aluminum oxide hydroxide on blocks of aluminum oxide after sliding tests. At high stresses, temperature fluctuations at contact points become high enough to form γ-Al_2O_3 from α-Al_2O_3. We do not know the RH at which a monolayer of water covers α-Al_2O_3 or γ-Al_2O_3, but in the presence of water, γ-Al_2O_3 is more easily hydroxylated than α-Al_2O_3, and a weak surface layer is created. This surface layer could deform plastically at contact junctions in the manner described by *Dieterich and Kilgore* [1994]. Thus we propose that the frictional behavior of alumina powder is dependent on contact area growth at water-weakened contact junctions. In both quartz and alumina powder experiments, the role of RH in sample consolidation appears minor compared to its role in contact junction strengthening processes.

4.2. Normal Stress Vibrations

[36] Compaction rates during vibrated SHS tests were approximately doubled and frictional healing was greater than in constant normal stress tests performed at the same RH. Thus there is either an additional healing mechanism associated with vibration or the normal stress vibrations enhance a single healing mechanism. We propose that there are two healing mechanisms present, one that is water-assisted and one that is strictly microstructural, perhaps due to consolidation and redistribution of localized shear (Figure 18). If true, then the healing present at 5% RH represents the effect of the normal stress vibrations, as there was negligible water-assisted healing observed for dry conditions under constant normal stress. We suggest that the microstructural healing is due to the redistribution of localized strain rate [*Sleep et al.*, 2000]. Because our layers have finite overall width, there is a practical limit to possible redistribution of strain rate. Therefore, healing rate would be expected to change when that limit is reached, in this case after 100 s vibration of double amplitude ~3.5 MPa (Figure 12).

[37] If healing measured at RH <5% is exclusively due to the redistribution of strain rate, then it may be subtracted from higher humidity healing to yield the purely water-assisted component of healing. We perform this operation on both constant normal stress and normal stress oscillation data at 45% RH and plot the double-difference data versus hold time (Figure 19). The slopes of the best fit lines are identical to within 1%, yielding the same water-assisted healing rates. Further, after subtracting out the 5% RH data, there is no slope change in the normal stress oscillation healing. We suggest that an offset on the log time axis occurs because the average contact junction lifetime is

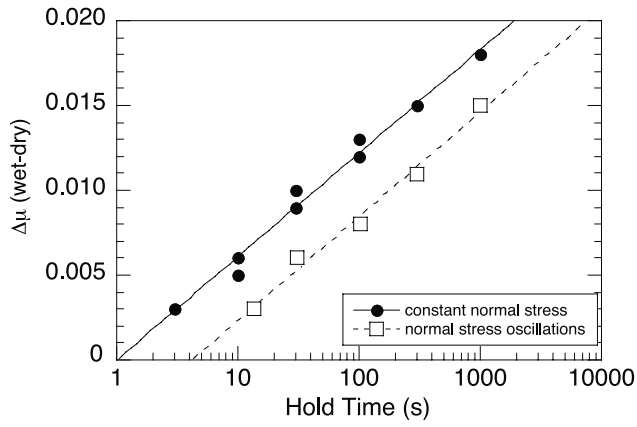

Figure 19. Frictional healing for the water-assisted mechanism. $\Delta\mu$ is determined by subtracting dry healing data (representing microstructural effects) from humid data (representing micromechanical plus contact junction strengthening). Data are shown for constant normal stress and vibrated SHS tests. Lines are best fit log linear healing rates and the slopes are the same to within 1%. We propose that vibrations reduce the average contact lifetime by a factor of 4 compared to constant normal stress SHS, resulting in an offset on the log time axis.

reduced by the enhanced consolidation (and particle movement) associated with normal stress vibration. Thus we favor the interpretation that two separate mechanisms cause healing in granular gouge: water-assisted strengthening of contact junctions and redistribution of strain rate throughout the granular layer, with the first being dominant in cases of negligible alteration of normal stress.

4.3. Friction Velocity Dependence

[38] We observe a transition from velocity strengthening to velocity weakening with increasing humidity for both quartz and alumina (Figure 15). Velocity dependence is in part a function of displacement: at 5 mm the layers exhibit velocity-strengthening behavior at all RHs and there is a transition to velocity weakening as shear becomes localized [*Marone*, 1998a; *Mair and Marone*, 1999]. After shear localization, rate-dependent behavior is strongly influenced by RH.

[39] SHS tests demonstrate that healing rate, and hence the empirical parameter b, increases with RH. This would be consistent with a transition in velocity dependence ($a-b$) from positive to negative values with increasing RH. However, it is important to note that examination of the raw velocity stepping data (Figures 14 and 15) and modeling (Figure 17) suggest that both the direct effect (parameter a) and evolution effect, b, change as a function of RH.

[40] The evolution distance, D_c, generally decreases with increasing RH for both quartz and alumina (Figure 17). The values of D_c at low humidity are of the same order as the mean grain size, indicating that the mechanisms controlling velocity dependence at low RH are acting at a scale larger than expected for contact junction processes. Thus we posit that in the absence of water, rate-dependency of friction is likely a function of reorganization mechanisms rather than contact junction processes. The width of the localized shear zone could be changing with RH, thus affecting D_c, however our layer thickness data are such that we cannot resolve this issue at present. The dilation term α, an indicator of shear band thickness [*Marone and Kilgore*, 1993], is greatest during velocity step tests at very low humidity. This is consistent with the view that shear localization is less developed at low RH, but the variation is comparable to calculated uncertainty.

5. Conclusions

[41] We have shown that humidity has a significant effect on frictional healing and velocity dependence for quartz and alumina powders at room temperature. We find a transition from velocity strengthening to velocity-weakening frictional behavior as RH increases. The transition occurs at 30–35% RH for quartz and 55–60% RH for alumina. Frictional healing is negligible at low humidity and increases with increasing RH for both the materials. The coefficient of sliding friction is independent of humidity.

[42] We observe that healing rate increases with increasing RH, consistent with *Dieterich and Conrad* [1984]. However, layer thickness change measured during SHS does not appear to correlate with the RH-dependence of healing data. We propose that dry SHS tests represent strictly microstructural healing and comparing tests with and without normal stress oscillation can isolate water-assisted healing operative at high-stress contact junctions.

[43] We interpret the dependence of healing on RH to be the result of chemically assisted mechanisms that strengthen contact junctions. Alumina forms a weak surface layer under high RH [*Gates et al.*, 1985] that may undergo time-dependent deformation. In quartz powder, if contact junctions were at the plastic yield stress, hydrolytic weakening would lead to greater asperity deformation and increased real area of contact. If asperities are in elastic contact, hydrogen bonding and desorption of water at the contact junction are two mechanisms that would provide a RH-dependent increase in quality of contact. Our observations are consistent with the view that rate and state friction effects in quartz derive from a thermally activated mechanism that operates at room temperature.

[44] **Acknowledgments.** We are grateful to S. Karner, K. Mair, and E. Richardson for scientific discussions. We benefited greatly from the comments and suggestions of associate editor G. Hirth and reviewers J. Rice and T. Tullis. This work was funded by National Science Foundation grants EAR-0001215 and EAR-0196570 and the Rosenblith Fellowship.

References

Beeler, N. M., T. E. Tullis, and J. D. Weeks, The roles of time and displacement in evolution effect in rock friction, *Geophys. Res. Lett.*, *21*, 1987–1990, 1994.

Blacic, J. D., and J. M. Christie, Plasticity and hydrolytic weakening of quartz single crystals, *J. Geophys. Res.*, *89*, 4223–4240, 1984.

Bocquet, L., E. Charlaix, S. Ciliberto, and J. Crassous, Moisture-induced ageing in granular media and the kinetics of capillary condensation, *Nature*, *396*, 735–737, 1998.

Boettcher, M., and C. Marone, Stability and strength of a laboratory shear zone under normal stress vibrations, *Eos Trans. AGU*, *82*(20), Spring Meet. Suppl., Abstract T61A-01, 2001.

Boitnott, G. N., R. L. Biegel, C. H. Scholz, N. Yoshioka, and W. Wang, Micromechanics of rock friction, 2, Quantitative modeling of initial friction with contact theory, *J. Geophys. Res.*, *97*, 8965–8978, 1992.

Bos, B., C. J. Peach, and C. J. Spiers, Frictional-viscous flow of simulated fault gouge caused by combined effects of phyllosilicates and pressure solution, *Tectonophysics*, *327*, 173–194, 2000.

Bowden, F. P., and D. Tabor, *The Friction and Lubrication of Solids*, Part 2, Clarenden, Oxford, England, 1964.

Chester, F. M., Effects of temperature on friction: Constitutive equations and experiments with quartz gouge, *J. Geophys. Res.*, *99*, 7247–7261, 1994.

Costin, L. S., Time-dependent deformation and failure, in *Fracture Mechanics of Rock*, edited by B. K. Atkinson, pp. 167–215, Academic, San Diego, Calif., 1987.

Crassous, J., E. Charlaix, and J.-L. Loubet, Capillary condensation between high-energy surfaces: An experimental study with a surface force apparatus, *Europhys. Lett.*, *28*(1), 37–42, 1994.

deGennes, P. G., Granular matter: A tentative view, *Rev. Mod. Phys.*, *71*(2), 374–382, 1999.

Dieterich, J. H., Time-dependent friction in rocks, *J. Geophys. Res.*, *77*, 3690–3697, 1972.

Dieterich, J. H., Time-dependent friction and the mechanics of stick-slip, *Pure Appl. Geophys.*, *116*, 790–805, 1978.

Dieterich, J. H., Modeling of rock friction, 1, Experimental results and constitutive equations, *J. Geophys. Res.*, *84*, 2161–2168, 1979.

Dieterich, J. H., and G. Conrad, Effect of humidity on time and velocity-dependent friction in rocks, *J. Geophys. Res.*, *89*, 4196–4202, 1984.

Dieterich, J. H., and B. Kilgore, Direct observation of frictional contacts: New insights for state-dependent properties, *Pure Appl. Geophys.*, *143*, 283–302, 1994.

Dieterich, J. H., and B. Kilgore, Imaging surface contacts: Power law contact distributions and stresses in quartz, calcite, glass and acrylic plastic, *Tectonophysics*, *256*, 219–239, 1996.

Dove, P. M., The dissolution kinetics of quartz in sodium chloride solutions at 25 degrees to 300 degrees C, *Am. J. Sci.*, *294*(6), 665–712, 1994.

Dove, P. M., and S. F. Elston, Dissolution kinetics of quartz in sodium chloride solutions; analysis of existing data and a rate model for 25 degrees C, *Geochim. Cosmochim. Acta*, *56*(12), 4147–4156, 1992.

Evans, B., and D. L. Kohlstedt, Rheology of rocks, in *Rock Physics and*

Phase Relations, A Handbook of Physical Constants, *AGU Ref. Shelf*, vol. 3, edited by T. J. Ahrens, pp. 148–165, AGU, Washington, D. C., 1995.
Evans, J. P., and F. M. Chester, Fluid-rock interaction in faults of the San Andreas system; inferences from San Gabriel Fault rock geochemistry and microstructures, *J. Geophys. Res.*, *100*, 13,007–13,020, 1995.
Gates, R. S., S. M. Hsu, and E. E. Klaus, Tribochemical mechanism of alumina with water, *Tribol. Trans.*, *32*, 357–363, 1989.
Geminard, J.-C., W. Losert, and J. P. Gollub, Frictional mechanics of wet granular material, *Phys. Rev. E*, *59*, 5881–5890, 1990.
Halsey, T. C., and A. J. Levine, How sandcastles fall, *Phys. Rev. Lett.*, *80*(14), 3141–3144, 1998.
Heslot, F., T. Baumberger, B. Perrin, B. Caroli, and C. Caroli, Creep, stick-slip, and dry-friction dynamics: Experiments and a heuristic model, *Phys. Rev. E*, *49*, 4973–4988, 1994.
Hirth, J. P., and J. R. Rice, On the thermodynamics of adsorption at interfaces as it influences decohesion, *Metall. Trans. A*, *11*, 1501–1511, 1980.
Hornbaker, D. J., R. Albert, I. Albert, A.-L. Barabasi, and P. Schiffer, What keeps sandcastles standing?, *Nature*, *387*, 765, 1997.
Iwamatsu, M., and K. Horii, Capillary condensation and adhesion of two wetter surfaces, *J. Colloid Interface Sci.*, *182*, 400–406, 1996.
Jaeger, H. M., S. R. Nagel, and R. P. Behringer, Granular solids, liquids and gases, *Rev. Mod. Phys.*, *68*(4), 1259–1273, 1996.
Jaoul, O., J. Tullis, and A. K. Kronenberg, The effect of varying water contents on creep behavior of Heavitree quartzite, *J. Geophys. Res.*, *89*, 4298–4312, 1984.
Karner, S. L., and C. Marone, Effects of loading rate and normal stress on stress drop and stick-slip recurrence interval, in *Geocomplexity and the Physics of Earthquakes*, *Geophys. Monogr. Ser.*, vol. 120, edited by J. B. Rundle, D. L. Turcotte, and W. Klein, pp. 187–198, AGU, Washington, D. C., 2000.
Karner, S. L., and C. Marone, Frictional restrengthening in simulated fault gouge: Effect of shear load perturbations, *J. Geophys. Res.*, *106*, 19,319–19,337, 2001.
Kronenberg, A. K., and J. Tullis, Flow strengths of quartz aggregates: Grain size and pressure effects due to hydrolytic weakening, *J. Geophys. Res.*, *89*, 4281–4297, 1984.
Mainprice, D. H., and M. S. Paterson, Experimental studies of the role of water in the plasticity of quartzites, *J. Geophys. Res.*, *89*, 4257–4270, 1984.
Mair, K., and C. Marone, Friction of simulated fault gouge for a wide variety of velocities and normal stresses, *J. Geophys. Res.*, *104*, 28,899–28,914, 1999.
Marone, C., Laboratory-derived friction laws and their application to seismic faulting, *Annu. Rev. Earth Planet. Sci.*, *26*, 696, 1998a.
Marone, C., The effect of loading rate on static friction and the rate of fault healing during the earthquake cycle, *Nature*, *391*, 69–72, 1998b.
Marone, C., and B. D. Kilgore, Scaling of the critical slip distance for seismic faulting with shear strain in fault zones, *Nature*, *362*, 618–621, 1993.
Marone, C., C. B. Raleigh, and C. H. Scholz, Frictional behavior and constitutive modeling of simulated fault gouge, *J. Geophys. Res.*, *95*, 7007–7025, 1990.
Martin, R. J., and W. B. Durham, Mechanisms of crack growth in quartz, *J. Geophys. Res.*, *80*, 4837–4844, 1975.
Michalske, T. A., and E. R. Fuller Jr., Closure and repropagation of healed cracks in silicate glass, *J. Am. Ceram. Soc.*, *68*, 5586–5590, 1985.
Mora, P., and D. Place, Numerical simulation of earthquake faults with gouge: Toward a comprehensive explanation for the heat flow paradox, *J. Geophys. Res.*, *103*, 21,067–21,089, 1998.
Morgan, J. K., Numerical simulations of granular shear zones using the distinct element method, 2, Effects of particle size distribution and interparticle friction on mechanical behavior, *J. Geophys. Res.*, *104*, 2721–2732, 1999.
Morgan, J. K., and M. S. Boettcher, Numerical simulations of granular shear zones using the distinct element method, 1, Shear zone kinematics and the micromechanics of localization, *J. Geophys. Res.*, *104*, 2703–2719, 1999.
Rabinowicz, E., The nature of static and kinetic coefficients of friction, *J. Appl. Phys.*, *22*, 1373–1379, 1951.
Rice, J. R., Hydrogen and interfacial cohesion, in *Effect of Hydrogen on Behavior of Materials*, edited by A. W. Thompson and I. M. Berstein, pp. 455–466, Metall. Soc. of AIME, New York, 1976.
Rice, J. R., N. Lapusta, and K. Ranjith, Rate and state dependent friction and the stability of sliding between elastically deformable solids, *J. Mech. Phys. Solids*, *49*, 1865–1898, 2001.
Richardson, E., and C. Marone, Effects of normal stress vibrations on frictional healing, *J. Geophys. Res.*, *104*, 28,859–28,878, 1999.
Ruina, A., Slip instability and state variable friction laws, *J. Geophys. Res.*, *88*, 10,359–10,370, 1983.
Sammis, C. G., G. King, and R. Biegel, The kinematics of gouge deformation, *Pure Appl. Geophys.*, *125*, 777–812, 1987.
Scholz, C. H., Earthquakes and friction laws, *Nature*, *391*, 37–42, 1998.
Scholz, C. H., and J. T. Engelder, The role of asperity indentation and ploughing in rock friction, I, Asperity creep and stick-slip, *Int. J. Rock Mech. Min. Sci.*, *13*, 149–154, 1976.
Segall, P., and J. R. Rice, Dilatancy, compaction, and slip instability of a fluid-infiltrated fault, *J. Geophys. Res.*, *100*, 22,155–22,171, 1995.
Sleep, N. H., Application of a unified rate and state friction theory to the mechanics of fault zones with strain localization, *J. Geophys. Res.*, *102*, 2875–2895, 1997.
Sleep, N. H., E. Richardson, and C. Marone, Physics of friction and strain rate localization in simulated fault gouge, *J. Geophys. Res.*, *105*, 25,875–25,890, 2000.
Teufel, L. W., and J. M. Logan, Effect of displacement rate on the real area of contact and temperatures generated during frictional sliding of Tennessee sandstone, *Pure Appl. Geophys.*, *116*, 840–865, 1977.
Thornton, C., Numerical simulations of deviatoric shear deformation of granular media, *Geotechnique*, *50*(1), 43–53, 2000.
Tullis, T. E., Rock friction constitutive behavior from laboratory experiments and its implications for an earthquake prediction field monitoring program, *Pure Appl. Geophys.*, *126*, 555–588, 1988.
Tullis, T. E., and J. D. Weeks, Constitutive behavior and stability of frictional sliding of granite, *Pure Appl. Geophys.*, *124*, 383–414, 1986.
Whalen, J. W., Thermodynamic properties of water adsorbed on quartz, *J. Phys. Chem.*, *65*, 1676–1681, 1981.
Wong, T.-F., Y. Gu, T. Yanagidani, and Y. Zhao, Stabilization of faulting by cumulative slip, in *Fault Mechanics and Transport Properties of Rocks; A Festschrift in Honor of W. F. Brace*, edited by B. Evans and T.-F. Wong, pp. 119–143, Academic, San Diego, Calif., 1992.

K. M. Frye, Department of Earth, Atmospheric, and Planetary Sciences, Massachusetts Institute of Technology, Cambridge, MA 02139, USA. (kfrye@mit.edu)

C. Marone, Department of Geosciences, Pennsylvania State University, 536 Deike Bldg, University Park, PA 16802, USA. (cjm38@psu.edu)